Low-sidelobe Imaging Method Utilizing Improved Spatially Variant Apodization for Forward-Looking Sonar

Lu Yan *, Juan Yang, Feng Xu, Shengchun Piao

Posted Date: 4 December 2023

doi: 10.20944/preprints202312.0150.v1

Keywords: forward-looking imaging sonar; spatially variant apodization; low-sidelobe; main lobe resolution; image quality

Article

Low-Sidelobe Imaging Method Utilizing Improved Spatially Variant Apodization for Forward-Looking Sonar

Lu Yan [1,*], Juan Yang [1], Feng Xu [1] and Shengchun Piao [2]

[1] Institute of Acoustics, Chinese Academy of Sciences, Beijing 100190, China; yangjuan@mail.ioa.ac.cn (J.Y.); xf@mail.ioa.ac.cn (F.X.)

[2] College of Underwater Acoustic Engineering, Harbin Engineering University, Harbin 150001, China; piaoshengchun@hrbeu.edu.cn

* Correspondence: yanlu@mail.ioa.ac.cn

Abstract: For two-dimensional forward-looking sonar imaging, high sidelobes significantly degrade the quality of sonar images. The cosine window function weighting method is often applied to suppress the sidelobe levels in the angular and range dimensions at the expense of the main lobe resolutions. Therefore, the improved spatially variant apodization imaging method for forward-looking sonar is proposed to reduce the sidelobes without degrading the main lobe resolution in angular-range dimensions. The proposed method is a nonlinear post-processing operation in which the raw complex-valued sonar image produced by a conventional beamformer and matched filter is weighted by a spatially variant coefficient. To enhance the robustness of the spatially variant apodization approach, the array magnitude and phase errors are calibrated to prevent beam sidelobe heightening from occurring prior to beamforming operations. The analyzed results of numerical simulations and a lake experiment demonstrate that the proposed method can greatly reduce the sidelobes to approximately -40 dB, while the main lobe width remains unchanged. Moreover, this method has an extremely simple computational process.

Keywords: forward-looking imaging sonar; spatially variant apodization; low-sidelobe; main lobe resolution; image quality

1. Introduction

Imaging sonars can directly present underwater scene information, which provides strong support for underwater target detection and recognition [1–3]. Imaging sonars can be divided by their detection coverage and system construction type: forward-looking [4], side-looking [5] and down-looking solutions [6]. In this paper, two-dimensional forward-looking sonar (FLS) is discussed, and a forward-looking sonar imaging method is proposed to reduce the sidelobes without sacrificing the main lobe resolution.

Generally, for FLS, the angular dimension is obtained by convention beamforming for a uniform linear array, and the range dimension is obtained by match filtering for a linear frequency modulated signal [7,8]. For the output envelopes of convention beamforming and match filtering, the main-to-side ratio of both is approximately -13dB[9,10]. Typically, in practical engineering, the ratio is needed to be approximately -40 dB to acquire high-quality sonar images. In practice, high sidelobe levels from a strong target echo can weaken or even completely mask the main lobe of a smaller target echo, so additional sidelobe suppression for FLS images is essential [11,12].

The conventional amplitude weighting cosine window functions are commonly applied to reduce the sidelobe level with angular and range dimensions for FLS, which may lead to the degradation of the angular and range resolutions. Compared with conventional beamforming, sonar images are obtained with lower sidelobe levels and narrower main lobe widths by utilizing adaptive beamforming (ADBF)[13–16]. Nevertheless, the performance of the ADBF methods degrades in the presence of array model mismatch due to imperfect array channels and inaccurately estimated data

 doi:10.20944/preprints202312.0150.v1

covariance matrices; hence, some robust adaptive beamforming algorithms have been researched. The calculation of the adaptive weighed vector in robust adaptive beamforming is equivalent to second-order cone programming problems, in which it has high complexity, and the prior knowledge of the programming problem is difficult to obtain due to the complicated underwater propagation [17]. Moreover, for forward-looking imaging sonar, these existing adaptive beamforming approaches are not applicable to the output in the range dimension. Thus, to obtain lower sidelobe levels, robust adaptive beamforming is difficult to use for forward-looking sonar imaging.

Compressive sensing (CS) has been proposed for use in arrays to improve the resolution of the spatial spectrum of underwater source locations in passive sonar. Compressed beamforming has also proven to be an effective approach for improving sonar image quality without increasing the array size [18–21]. Additionally, a few transducers can be implemented in compressed beamforming to obtain a similar image quality to that produced by a larger-aperture array. Nevertheless, the performance of CS in underwater acoustics imaging will be limited since the prior knowledge cannot be properly matched to the reverberation-rich scenes of underwater environments.

Deconvolution algorithms are proposed to improve the angular resolution in spatial spectrum estimation by processing the beamformers' output data. Then, the methods are extended to high-frequency sonar imaging to achieve higher resolution in both the angular and range dimensions simultaneously [7,8,12,22–27]. However, the deconvoluted results require several iterations, and the performance is related to the number of iterations. Thus, the method is difficult to apply in engineering due to the higher computational complexity.

The spatially variant apodization (SVA) method is proposed and applied for synthetic aperture radar (SAR) imaging. In this method, the properties of the cosine-on-pedestal weighing functions are utilized to achieve range dimension sidelobe suppression without broadening the main lobe[28–31]. Furthermore, it is regarded as a post-processing method with a lower computational cost in the image domain. Moreover, it can reserve the raw sonar image. However, the principle of SAR imaging is different from that of multibeam imaging sonar, so the SVA method cannot be directly applied to imaging sonar sidelobe reduction. The desired array point spread function (PSF) of imaging sonar is space-invariant; thus, from this viewpoint, the SVA method is suitable for underwater acoustic imaging. Nevertheless, the SVA method is rarely reported in the sonar imaging field, and the original SVA method is less robust to existing array amplitude phase errors.

To obtain lower sidelobe levels without degrading the main lobe resolution in angular-range dimensions, an improved spatially variant apodization forward-looking sonar imaging method is proposed in this article. The proposed method is a nonlinear post-processing operation in which the raw complex-valued sonar image data produced by a conventional beamformer and matched filter are weighted by a spatially variant coefficient. To enhance the robustness of the spatially variant apodization approach, the array magnitude and phase errors are calibrated to avoid beam sidelobe heightening prior to beamforming operations. The analyzed results of the numerical simulations and a lake experiment demonstrate that the proposed method can greatly reduce the sidelobes to approximately -40 dB on the premise of the main lobe width remaining unchanged. Moreover, this method has an extremely simple computational process.

The paper is organized as follows. In Section 2, the conventional forward-looking sonar imaging procedure is described. The improved forward-looking sonar imaging method, which utilizes spatially variant apodization combined with array magnitude and phase error calibration, is described in Section 3. Analyses of the simulation and lake experiment results are presented to demonstrate the effectiveness of the proposed approach in Section 4. In Section 5, the conclusions are provided.

2. Conventional Variant Apodization for Forward-Looking Sonar Imaging

In this section, the signal model of forward-look imaging sonar is first described. Then, conventional variant apodization methods are introduced.

Preprints (www.preprints.org) | NOT PEER-REVIEWED | Posted: 4 December 2023 doi:10.20944/preprints202312.0150.v1

2.1. Signal Model

We assume that forward-looking imaging sonar is composed of a single transmitter and a receiving uniform linear array (ULA) with N elements at a half-wavelength spacing. For simplicity, the narrowband far-field underwater targets are assumed to be ideal point scatterers. The transmission loss and the medium absorption loss associated with the free-space propagation are neglected, and the underwater reverberations and noise are ignored.

For a target, the discrete baseband superposed echo received by the n *th* receiver can be written as follows:

$$\boldsymbol{x}_n(t)=\sigma_0 s_0(t)\exp(-\mathrm{j}2\pi f_0\tau_n) \tag{1}$$

where σ_0 denotes the complex backscattering coefficient of the target and $s_0(t)$ denotes the envelope of the transmitted waveforms. τ_n is the propagation delay time between the scatterer and the n *th* receiver, and f_0 denotes the carrier frequency. The transmitted linear modulated frequency (LFM) waveforms are expressed as follows:

$$s_0(t)=\mathrm{rect}\left(\frac{t}{T}\right)\exp\left[\mathrm{j}2\pi\left(-\frac{B}{2}t+\frac{1}{2}\frac{B}{T}t^2\right)\right]\exp\left(\mathrm{j}2\pi f_0 t\right) \tag{2}$$

where $\mathrm{rect}(\bullet)$ denotes the rectangular window function, and B and T represent the bandwidth and the chirp duration, respectively.

The time-domain conventional beamforming (CBF) output is given by

$$\begin{aligned} y_q(t)&=\sum_{n=1}^{N} w_n^* x_n(t)\\ &=\sigma_0 s_0(t)\sum_{n=1}^{N} w_n^*\exp(-\mathrm{j}2\pi f_0\tau_n) \end{aligned} \tag{3}$$

where w_n denotes the complex weight, $w_n=\exp[-\mathrm{j}2\pi f_0 nd\sin\theta_0/c]/\sqrt{N}$, d represents the spacing between adjacent receiving elements, $(\bullet)^*$ denotes the conjugate, θ_0 denotes the beam pointing, and c is the sound speed underwater. Then, the beamforming complex output can be expressed as follows:

$$y_q(t)=\sigma_0 s_0(t)\frac{\mathrm{sinc}\left[\dfrac{\pi Nd\left(u_\theta-u_{\theta 0}\right)}{\lambda}\right]}{\mathrm{sinc}\left[\dfrac{\pi d\left(u_\theta-u_{\theta 0}\right)}{\lambda}\right]}=\sigma_0 s_0(t)BP(u_\theta) \qquad -1\le u_\theta\le 1 \tag{4}$$

where $u_\theta=\sin\theta$, $\mathrm{sinc}(x)=\dfrac{\sin x}{x}$, λ is the wavelength, and $BP(u_\theta)$ denotes the array beampattern expressing the PSF in the angular dimension of sonar images. Equation (4) indicates that the angular dimension of the sonar image is only related to the angle[9].

In the range dimension of the sonar image, assuming that the angular dimension and range dimension are independent of each other, the matched filter output envelope of the q *th* beam can be expressed as follows:

$$z_{Bq}(t)=\sigma_0 T\frac{\sin\pi B(1-\frac{|t|}{T})t}{\pi Bt}\mathrm{rect}(\frac{t}{2T})=\sigma_0\boldsymbol{R}(t) \tag{5}$$

when t is less than or equal to T, $\boldsymbol{R}(t)$ is approximated as

Preprints (www.preprints.org) | NOT PEER-REVIEWED | Posted: 4 December 2023 doi:10.20944/preprints202312.0150.v1

$$\boldsymbol{R}(t) = T\mathrm{sinc}(\pi Bt)\mathrm{rect}(\frac{t}{2T}) \tag{6}$$

where $\boldsymbol{R}(t)$ denotes the PSF in the range dimension of sonar images. Equation (6) indicates that the envelope of the matched filter output approximately follows the sinc function. Therefore, the sidelobe levels are high in two dimensions of the sonar images.

Sidelobe reduction is accomplished via amplitude weighting applied angular dimension echoes or range dimension echoes, and the cosine-on-pedestal weighting functions are expressed as follows:

$$\begin{aligned} w(n) &= 1 + 2w\cos(\frac{2\pi n}{N-1}) \\ &= 1 + we^{(\mathrm{j}\frac{2\pi n}{N-1})} + we^{(-\mathrm{j}\frac{2\pi n}{N-1})},\ 0 \le w \le 1/2, n = -(N-1)/2, \cdots, 0, \cdots, (N-1)/2 \end{aligned} \tag{7}$$

Similarly, any unweighted sonar image angular-range dimension sidelobe can be suppressed using one of the families of the cosine-on-pedestal weighting functions. However, lower sidelobes have been achieved at the expense of the main lobe width by cosine-on-pedestal weighting functions.

2.2. Dual apodization and multi-apodization

To suppress sidelobe levels while preserving the main lobe resolution, nonlinear apodization operators are proposed, i.e., dual and multi-apodizations. For simplicity of analysis, since there is only a scatter in the echoes, the beampattern is used to calculate the azimuth beamforming output.

Taking the angular dimension beampattern of imaging sonar as an example, the dual apodization (DA) method calculates the beampattern of the receiving array by using two window functions, one using rectangular window processing and the other using cosine or Chebyshev window processing. Then, at each spatial sampling point, the minimum value of the two processing responses is selected as the final response output value. DA calculation processing is expressed as follows:

$$\tilde{\boldsymbol{B}}_{DA}(u_{\theta i}) = \min\left[\left|\boldsymbol{B}_{w1}(u_{\theta i})\right|, \left|\boldsymbol{B}_{w2}(u_{\theta i})\right|\right] \quad i = 1,2,3,\cdots,M_{u_\theta} \tag{8}$$

where $\boldsymbol{B}_{w1}(u_{\theta i})$ represents the beamforming complex output obtained by using uniform weighting, and $\boldsymbol{B}_{w2}(u_{\theta i})$ represents the beamforming complex output obtained by using Hanning window weighting.

DA can be extended to tri-apodization (TA) by window function weighting, and the output result of TA can be obtained by repeating the above steps. Then, TA calculation processing can be expressed as follows:

$$\tilde{\boldsymbol{B}}_{TA}(u_{\theta i}) = \min\left[\left|\boldsymbol{B}_{w1}(u_{\theta i})\right|, \left|\boldsymbol{B}_{w2}(u_{\theta i})\right|, \left|\boldsymbol{B}_{w3}(u_{\theta i})\right|\right] \quad i = 1,2,3,\cdots,M_{u_\theta} \tag{9}$$

where $\boldsymbol{B}_{w3}(u_{\theta i})$ represents the beamforming complex output obtained by using the Hamming window weighting calculation. We consider a ULA consisting of 48 array elements, where the spacing between adjacent array elements is a half wavelength. The beampatterns obtained by using uniform weighting, Hanning window weighting, Hamming window weighting, DA and TA are shown in Figure 1. Evidently, DA and TA have narrow main lobe widths of the sinc function and small sidelobes of the cosine window function. However, with the larger numbers of weighting functions, it still does not reach the ideal sidelobe levels, and these methods only make use of the amplitude information of the beampattern, ignoring the complex information[29].

Preprints (www.preprints.org) | NOT PEER-REVIEWED | Posted: 4 December 2023 doi:10.20944/preprints202312.0150.v1

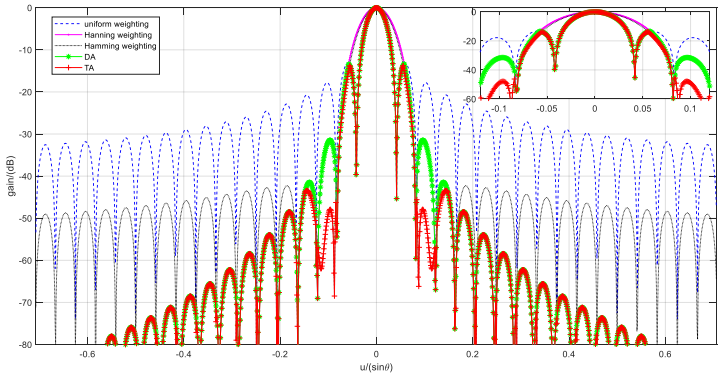

Figure 1. Comparison of the beampatterns with different weighing methods.

The complex DA (CDA) method makes full use of the amplitude and sign information of the real part and the imaginary part of the beamforming output. In the main lobe region, the sign of the uniform weighting real part (imaginary part) is the same as that of the cosine window weighted real part (imaginary part). In the sidelobe region, the sign of the uniform weighting real part (imaginary part) is opposite to that of the cosine window weighted real part (imaginary part); then, the processing method of CDA is expressed as:

$$\boldsymbol{I}_{cda}(u_{\theta i}) = \begin{cases} 0, & \boldsymbol{I}(u_{\theta i})\boldsymbol{I}_w(u_{\theta i}) < 0 \\ \min(\left|\boldsymbol{I}(u_{\theta i})\right|, \left|\boldsymbol{I}_w(u_{\theta i})\right|), & \text{others} \end{cases} \tag{10}$$

where $\boldsymbol{I}(u_{\theta i})$ represents the real part of the uniform weighting beamforming output and $\boldsymbol{I}_w(u_{\theta i})$ represents the real part of the cosine base window function weighting beamforming output. Moreover, the imaginary part can be determined with Equation (10). The simulation conditions are the same as in Figure 1, and the beam pattern response with different weighting processing is shown in Figure 2.

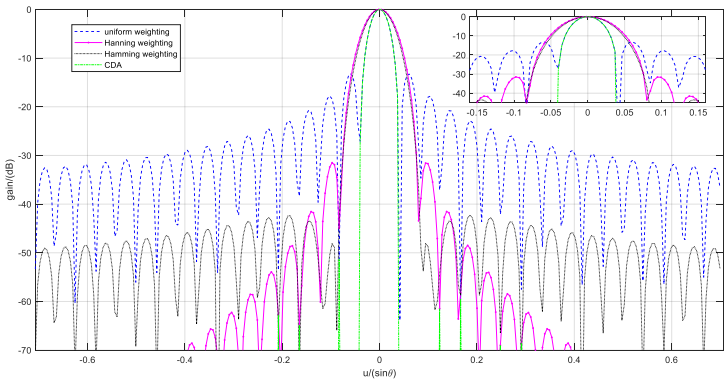

Figure 2. Comparison of the beam patterns with different weighing methods.

As seen from Figure 2, compared with other weighting methods, CDA obtains significantly lower sidelobes below approximately -40 dB without degrading the main lobe resolution, and it has the advantages of simplicity and easy implementation.

Similarly, the matched filter output in the range dimension also reduces sidelobes by using CDA at each time sampling. Considering the LFM signal bandwidth of 8 kHz and pulse width of 10 ms, there is a single target point, and simulation results with different weighting methods are shown in Figure 3. Obviously, the matched filter output has lower sidelobe levels of less than -40 dB without decreasing the main lobe resolution.

Preprints (www.preprints.org) | NOT PEER-REVIEWED | Posted: 4 December 2023 doi:10.20944/preprints202312.0150.v1

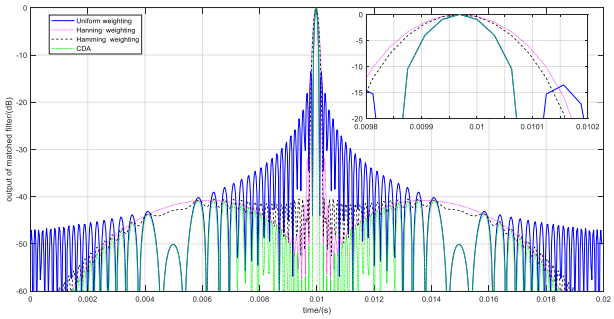

Figure 3. Output of the matched filter with different weighing methods.

CDA has a dramatic positive impact on the visual appearance of sonar images in two dimensions but at the expense of an increased computational burden. Additionally, the envelope of the PSF deviates from the theoretical value; thus, such methods are less robust to existing array amplitude phase errors.

3. Improved spatially variant apodization forward-looking sonar imaging method

Sidelobe improvements can be achieved by using cosine window weighting, which decreases the main lobe resolution. DA and multi-apodization can be performed to obtain a narrow main lobe, while these methods can also simultaneously achieve improved sidelobes if larger numbers of weighting windows are used. Furthermore, the CDA method achieves lower sidelobes of approximately -40 dB, while also preserving the main lobe resolution. However, this method has a higher computational complexity and is less robust. Thus, the improved SVA forward-looking sonar imaging algorithm is proposed to reduce the sidelobes without degrading the main lobe resolution in angular-range dimensions.

The proposed method is a nonlinear post-processing operation in which the raw complex-valued sonar image produced by a conventional beamformer and matched filter is weighted by a spatially variant coefficient. To enhance the robustness of the spatially variant apodization approach, the array magnitude and phase errors are calibrated to avoid beam sidelobe heightening prior to the beamforming operation. The analyzed results of numerical simulations and a lake experiment demonstrate that the proposed method can greatly reduce the sidelobes to approximately -40 dB and simultaneously maintain the main lobe width. Furthermore, this method is extremely simple computationally.

3.1. SVA for two-dimensional forward-looking sonar imaging

To preserve the main lobe width and suppress the sidelobes, the SVA exploits the sinc function characteristics and the special properties of raised-cosine weighting functions, which allows each spatial-time sampling location in a sonar image to use its amplitude weighting function.

By combining the expression of cosine-on-pedestal weighting window functions (7) with the beamforming output (3), the beamforming output with cosine-on-pedestal weighting can be expressed as follows:

Preprints (www.preprints.org) | NOT PEER-REVIEWED | Posted: 4 December 2023 doi:10.20944/preprints202312.0150.v1

$$
\begin{aligned}
\boldsymbol{B}_s(u_\theta) &= \frac{1}{N}\sum_{n=-(N-1)/2}^{(N-1)/2}[1+w\mathrm{e}^{\mathrm{j}\frac{2\pi n}{N-1}}+w\mathrm{e}^{-\mathrm{j}\frac{2\pi n}{N-1}}]^* e^{\mathrm{j}nd\frac{2\pi}{\lambda}u_\theta} \\
&= \frac{1}{N}\sum_{n=-(N-1)/2}^{(N-1)/2} e^{\mathrm{j}nd\frac{2\pi}{\lambda}u_\theta} + \frac{1}{N}w\sum_{n=-(N-1)/2}^{(N-1)/2}\mathrm{e}^{\mathrm{j}2n\pi(\frac{du_\theta}{\lambda}+\frac{1}{N-1})} + \frac{1}{N}w\sum_{n=-(N-1)/2}^{(N-1)/2}\mathrm{e}^{\mathrm{j}2n\pi(\frac{du_\theta}{\lambda}-\frac{1}{N-1})} \\
&= \frac{\mathrm{sinc}\left(\frac{Ndu_\theta}{\lambda}\right)}{\mathrm{sinc}\left(\frac{du_\theta}{\lambda}\right)} + w\frac{\mathrm{sinc}\left(\frac{Ndu_\theta}{\lambda}+\frac{N}{N-1}\right)}{\mathrm{sinc}\left(\frac{du_\theta}{\lambda}+\frac{1}{N-1}\right)} + w\frac{\mathrm{sinc}\left(\frac{Ndu_\theta}{\lambda}-\frac{N}{N-1}\right)}{\mathrm{sinc}\left(\frac{du_\theta}{\lambda}-\frac{1}{N-1}\right)} \\
&= \frac{\mathrm{sinc}\left(\frac{Ndu_\theta}{\lambda}\right)}{\mathrm{sinc}\left(\frac{du_\theta}{\lambda}\right)} + w\frac{\mathrm{sinc}\left[\frac{Nd}{\lambda}\left(u_\theta+\frac{\lambda}{d(N-1)}\right)\right]}{\mathrm{sinc}\left[\frac{d}{\lambda}\left(u_\theta+\frac{\lambda}{d(N-1)}\right)\right]} + w\frac{\mathrm{sinc}\left[\frac{Nd}{\lambda}\left(u_\theta-\frac{\lambda}{d(N-1)}\right)\right]}{\mathrm{sinc}\left[\frac{d}{\lambda}\left(u_\theta-\frac{\lambda}{d(N-1)}\right)\right]}
\end{aligned}
\tag{11}
$$

With reference to Equation (4), Equation (11) can be expressed as follows:

$$
\boldsymbol{B}_s(u_\theta)=\boldsymbol{B}(u_\theta)+w\boldsymbol{B}(u_\theta+\frac{\lambda}{d(N-1)})+w\boldsymbol{B}(u_\theta-\frac{\lambda}{d(N-1)}) \tag{12}
$$

According to Equation (12), the beamforming output weighted by cosine-on-pedestal functions is equivalent to the superposition of the conventional beamforming output uniform weighting and weighted shifted conventional beamforming output uniform weighting, in which the beam domain data are complex data composed of real and imaginary parts, i.e., $\boldsymbol{B}_s(u_\theta)=\boldsymbol{I}_s(u_\theta)+\mathrm{j}\boldsymbol{Q}_s(u_\theta)$.

To effectively suppress the beam sidelobes, the SVA algorithm attempts to estimate the optimal solution w for each special location. The real and imaginary parts of the beam domain data cannot be used to obtain the minimum value when $\boldsymbol{B}_s(u_\theta)$ is being simultaneously and directly calculated. However, the real and imaginary parts can be separately calculated. Then, the minimum value of the real part can be solved under the constraint of the $|\boldsymbol{I}_s(u_\theta)|^2$ minimum of the real part, and the minimum value of the imaginary part can be solved in the same way. Then, the minimum value of the beam domain data can be obtained.

In the angular dimension, sample points in the beam domain are used as variables to represent the beam domain data.

$$
\boldsymbol{B}_s(m)=\boldsymbol{B}(m)+w(m)\boldsymbol{B}(m+k_a)+w(m)\boldsymbol{B}(m-k_a) \tag{13}
$$

where k_a denotes the shift sampling numbers and be calculated with $k_a=\left\lfloor\frac{\lambda}{d_B(N-1)d}\right\rfloor$. In practical applications, $k_a\le 10$. d_B is the u_θ spacing of adjacent beams, $\lfloor\bullet\rfloor$ denotes the downward integer operation, and $\boldsymbol{B}_s(m)=\boldsymbol{I}_s(m)+\mathrm{j}\boldsymbol{Q}_s(m)$, $\boldsymbol{B}(m)=\boldsymbol{I}(m)+\mathrm{j}\boldsymbol{Q}(m)$. For the real part of the beam domain data, the minimum $|\boldsymbol{I}_s(m)|^2$ subject to $0\le w_I(m)\le 1/2$ is applied in the SVA algorithm to estimate the optimal solution $w_I(m)$, which is expressed as follows:

$$
\begin{cases}
\min\limits_{w_I(m)}\left\{|\boldsymbol{I}_s(m)|^2\right\} \\
\text{s.t.}\quad 0\le w_I(m)\le 1/2
\end{cases}
\tag{14}
$$

The solution of $w_I(m)$ is obtained by setting the partial derivative of $|\boldsymbol{I}_s(m)|^2$ equal to zero with respect to $w_I(m)$ and $\partial|\boldsymbol{I}_s(m)|^2/\partial w_I(m)=0$. Additionally, $w_I(m)$ can be determined as follows:

$$
w_I(m)=\frac{-\boldsymbol{I}(m)}{\boldsymbol{I}(m+1)+\boldsymbol{I}(m-1)} \tag{15}
$$

Preprints (www.preprints.org) | NOT PEER-REVIEWED | Posted: 4 December 2023 doi:10.20944/preprints202312.0150.v1

By inserting Equation (15) into Equation (13) and combining the properties of the CDA method, the output beam domain of the sonar image by SVA can be written as follows:

$$\boldsymbol{I}_s(m)=\begin{cases}\boldsymbol{I}(m), & w_I(m)<0\\ 0, & 0\le w_I\le 1/2\\ \boldsymbol{I}(m)+(1/2)[\boldsymbol{I}(m+k)+\boldsymbol{I}(m-k)], & w_I(m)>1/2\end{cases} \tag{16}$$

Equation (16) is also performed on the imaginary part independently, and $w_Q(m)$ and $\boldsymbol{Q}_s(m)$ are achieved. Therefore, the beam domain SVA algorithm applies the optimal weight at the sampling point of each beam on the condition of minimization of $|\boldsymbol{I}_s(m)|^2$ and $|\boldsymbol{Q}_s(m)|^2$ independently. Thus, the main lobe of the beam can be preserved, and the sidelobe of the beam can be suppressed.

To further simplify the computational burden, assuming $\boldsymbol{I}_a(m)=(1/2)[\boldsymbol{I}(m+k)+\boldsymbol{I}(m-k)]$, and combined with Equation (15), the beam domain SVA algorithm can also be expressed as follows:

$$\boldsymbol{I}_s(m)=\begin{cases}\boldsymbol{I}(m), & \boldsymbol{I}_a(m)\boldsymbol{I}(m)\ge 0\\ 0, & \boldsymbol{I}_a(m)\boldsymbol{I}(m)<0\ \&\ |\boldsymbol{I}(m)|<|\boldsymbol{I}_a(m)|\\ \boldsymbol{I}(m)+\boldsymbol{I}_a(m), & \text{else}\end{cases} \tag{17}$$

Assuming that $\boldsymbol{I}(m)$ is within a main lobe, $\boldsymbol{I}(m)$ and $\boldsymbol{I}_a(m)$ have the same signs, $\boldsymbol{I}_a(m)\boldsymbol{I}(m)\ge 0$, i.e., the beam main lobes are preserved. When $\boldsymbol{I}(m)$ is within an area of pure sidelobes, $\boldsymbol{I}(m)$ and $\boldsymbol{I}_a(m)$ have opposite signs, and $|\boldsymbol{I}(m)|<|\boldsymbol{I}_a(m)|$, i.e., the beam sidelobes are completely suppressed. Assuming that $\boldsymbol{I}(m)$ is in an area of a beam main lobe superimposed with beam sidelobes, $\boldsymbol{I}(m)$ and $\boldsymbol{I}_a(m)$ have opposite signs and $|\boldsymbol{I}(m)|>|\boldsymbol{I}_a(m)|$, i.e., the beam domain data are suppressed somewhat in an attempt to reduce the impact of the beam sidelobes. Moreover, the real and imaginary parts of the SVA algorithm are equivalent to those of the CDA algorithm.

Since the output envelope matching filter in the range dimension is also in the form of a sinc function, lower sidelobes can be achieved, while the main lobe resolution can be preserved by using the SVA algorithm.

The effects of the frequency domain cosine window weighting and time domain cosine window weighting for distance sidelobe reduction is basically the same. Furthermore, combined with the property of the Fourier transform, the matching template of the frequency domain window functions can be represented as follows:

$$H'(f)=\boldsymbol{w}(f)\boldsymbol{s}^*(f) \tag{18}$$

where $\boldsymbol{w}(f)$ is the cosine base window function with respect to f, and $\boldsymbol{s}(f)$ is the frequency domain of the transmitted pulse signal. Thus, the matched filter output using the frequency domain window weighting can be expressed as follows:

$$\begin{aligned}\boldsymbol{R}'(f)&=\boldsymbol{s}(f)\boldsymbol{H}'(f)=\boldsymbol{s}(f)\left[\boldsymbol{s}^*(f)\boldsymbol{w}(f)\right]\\ &=\boldsymbol{s}(f)\boldsymbol{s}^*(f)\left[1+w\mathrm{e}^{(\mathrm{j}\frac{2\pi f}{B})}+w\mathrm{e}^{(-\mathrm{j}\frac{2\pi f}{B})}\right]\\ &=\boldsymbol{R}(f)+\boldsymbol{R}(f)w\mathrm{e}^{(\mathrm{j}\frac{2\pi f}{B})}+\boldsymbol{R}(f)w\mathrm{e}^{(-\mathrm{j}\frac{2\pi f}{B})}\end{aligned} \tag{19}$$

Equation (19) is transferred to the time domain.

$$\boldsymbol{R}'(t)=\boldsymbol{R}(t)+\boldsymbol{R}(t+1/B)+\boldsymbol{R}(t-1/B) \tag{20}$$

According to Equation (20), the matched filter output weighted by cosine-on-pedestal functions is equivalent to the superposition of the conventional matched filter output uniform weighting and weighted shifted conventional matched filter output uniform weighting. Then, the sonar image range dimension discrete output by SVA can be expressed as follows:

Preprints (www.preprints.org) | NOT PEER-REVIEWED | Posted: 4 December 2023 doi:10.20944/preprints202312.0150.v1

$$\boldsymbol{R}_s(p)=\boldsymbol{R}(p)+w\boldsymbol{R}(p+k_r)+w\boldsymbol{R}(p-k_r) \tag{21}$$

where p represents the samples in the range dimensions, k_r denotes the shift sampling numbers, $k_r=\left\lfloor \frac{1}{T_s B} \right\rfloor$, and T_s is the sampling rate time domain of the echoes.

According to the above derivation, we proposed a two-step SVA algorithm in which sonar imaging is first applied to the angular dimension and then applied it to the range dimension. This process achieves the sonar imaging effect with angular-range sidelobe suppression, while preserving the angular-range resolution.

3.2. Amplitude and phase error calibration

In practical engineering, the magnitude and phase errors of sonar arrays always exist due to the non-ideal statuses. In this case, it causes sidelobe heightening, resulting in the output envelope of angular-range dimensions deviating from theoretical values. Thus, the SVA algorithm is less robust, and the array amplitude and phase inconsistencies should be calibrated before using the SVA algorithm.

The array phase difference ψ_n represents the measured phase difference that is the sum of the additional phase shift φ_n caused by array channel nonuniformity and the geometric phase difference ϕ_n caused by the sound path difference, i.e., $\psi_n=\phi_n+\varphi_n$.

In practice, the geometric phase difference ϕ_n can be calculated on the basis of the sonar array parameters. Assuming that a sound source is located at the (r_s,θ_s) near field, the additional phase shift φ_n can be calibrated by minimizing an appropriate cost function as follows:

$$\Upsilon=\min_{r_s,\theta_s}\left[\sum_{n=1}^{N}[\hat{\psi}_n-\frac{2\pi}{\lambda}(r_n-r_s)]^2\right] \tag{22}$$

where r_n is the distance between the sound source and the *n th* receiver. Equation (22) is estimated by adopting least squares of the phase difference, and when the Υ value is the minimum, the location of the source can be precisely estimated. Within the preset position range of the sound source, the minimum value has unique convergence, that is:

$$\begin{cases}\dfrac{\partial\Upsilon}{\partial r}=0\\ \dfrac{\partial\Upsilon}{\partial\theta}=0\end{cases} \tag{23}$$

Then, the additional phase shift of the *n th* receiver φ_n can be obtained as follows:

$$\hat{\varphi}_n=\hat{\psi}_n-\frac{2\pi}{\lambda}\left\{[\hat{r}_s^2+d_n^2-2\hat{r}_s d_n\sin\hat{\theta}_s]^{1/2}-\hat{r}_s\right\} \tag{24}$$

where $\hat{\theta}_s$ and $\hat{r}_s$ are the angle and range of the sound source estimated by Equation (22), respectively. To improve the measurement accuracy of the phase difference, phase inconsistencies are usually measured and calculated on multiple angles of the sound source.

Multiple samples of the sound source direct wave signal received by each element are averaged, and the amplitude of each element is estimated as follows:

$$A_n=\frac{1}{K}\sum_{i=1}^{K}\left|x_n(t_i)\right| \tag{25}$$

where K denotes the number of samples. The amplitude of the reference matrix element is subtracted to obtain the amplitude inconsistency.

Preprints (www.preprints.org) | NOT PEER-REVIEWED | Posted: 4 December 2023 doi:10.20944/preprints202312.0150.v1

According to the estimated phase inconsistency $\hat{\varphi}_n$ and the amplitude inconsistency $\Delta\hat{A}_n$ between array elements, the array amplitude and phase inconsistency calibrated matrix can be expressed as follows:

$$\hat{\boldsymbol{\Gamma}} = \mathrm{diag}\left[\frac{1}{(1+\Delta\hat{A}_1)}e^{-\mathrm{j}\Delta\hat{\varphi}_1}, \frac{1}{(1+\Delta\hat{A}_2)}e^{-\mathrm{j}\Delta\hat{\varphi}_2}, \frac{1}{(1+\Delta\hat{A}_n)}e^{-\mathrm{j}\Delta\hat{\varphi}_n}, \cdots, \frac{1}{(1+\Delta\hat{A}_N)}e^{-\mathrm{j}\Delta\hat{\varphi}_N}\right] \tag{26}$$

where $\hat{\boldsymbol{\Gamma}}$ compensates for the beamforming weighting vector. The amplitude and phase errors in the range dimension are ignored here due to the complicated underwater propagation environment, and further research will be conducted in the future.

In the proposed method, the amplitude and phase inconsistency is first calibrated. Then, a two-step SVA is applied to the azimuth-range dimensions. Therefore, the sidelobe levels are suppressed without sacrificing the main lobe resolution by the improved SVA algorithm for forward-looking sonar imaging, which is extremely simple computationally and has better robustness.

4. Simulation and Experimental Results

In this section, we mainly analyze sonar single-ping imaging where the conventional method, CDA method and proposed improved SVA method are employed, and a comparative study is conducted via simulations and a lake experiment.

4.1. Simulation results

4.1.1. Analysis of the resolutions and sidelobes

A ULA spacing half wavelength with elements from 40 to 200 is considered. The beam main lobe widths and peak sidelobe levels versus the number of receivers are investigated by uniform weighting, Hamming weighting, CDA and SVA. The corresponding results are given in Figure 4 and Figure 5, respectively.

Obviously, the beam main lobe widths of CDA and SVA are both consistent with the uniform weighting method with 40 to 200 receivers. Meanwhile, the beam peak sidelobe levels (PSLs) of CDA and SVA are both lower by -40 dB, whereas the PSL of the uniform weighting method is approximately -13 dB. However, the sidelobe levels are reduced with a degrading main lobe resolution via Hamming weighting.

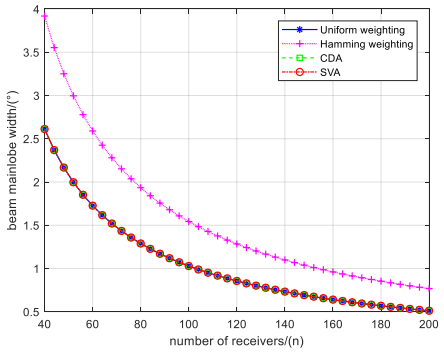

Figure 4. Beam width versus the number of receivers.

Preprints (www.preprints.org) | NOT PEER-REVIEWED | Posted: 4 December 2023 doi:10.20944/preprints202312.0150.v1

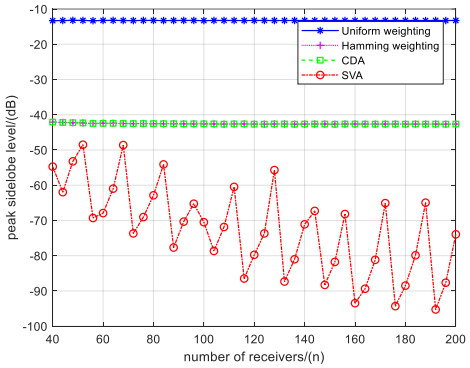

Figure 5. Peak sidelobe level versus the number of receivers.

Since the carrier frequency of the imaging sonar is 80 kHz, the transmitted signal is a linear frequency modulation signal. Additionally, the pulse width is 40 ms, and the bandwidth changes from 5 kHz to 20 kHz. The outputs of matched filtering are obtained by using uniform weighting, Hamming window weighting, CDA processing, and SVA processing methods. The simulation results of the main lobe width and the peak sidelobe level are shown in Figure 6 and Figure 7, respectively.

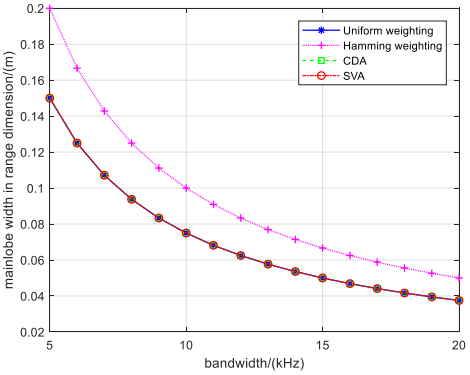

Figure 6. Range dimension main lobe width versus bandwidth. .

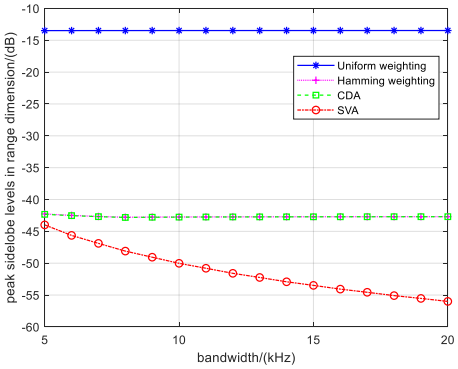

Figure 7. Range dimension peak sidelobe level versus bandwidth.

From Figure 6 and Figure 7, it is shown that the main lobe width of the target point in the range dimension is related to the bandwidth of the transmitted signal, where the main lobe width obtained by the SVA method is consistent with the conventional method and consistent with the theoretical value, e.g., when the bandwidth is 10 kHz, the main lobe width is 0.075 m. In the bandwidth range of 8 kHz to 20 kHz, the main lobe and sidelobe ratios obtained by using the conventional method are approximately 13 dB, while the main lobe and sidelobe ratios obtained by the SVA method are

Preprints (www.preprints.org) | NOT PEER-REVIEWED | Posted: 4 December 2023 doi:10.20944/preprints202312.0150.v1

approximately 40 dB. Furthermore, the range dimension SVA method can also achieve lower sidelobe levels while maintaining the same main lobe width.

4.1.2. Analysis of the array gain

The improvement of the output signal noise ratio (SNR) between the SVA method and CBF beamforming is estimated analytically by adopting the array directivity index, which is defined as the array gain in isotropic noise in the following equation:

$$\mathrm{AG}_{\mathrm{sva}}=10\log_{10}\left(\frac{2}{\int_{-1}^{1}B_{p\_sva}^{2}(u_{\theta})du_{\theta}}\right) \tag{27}$$

where $B_{p\_sva}^{2}(u_{\theta})$ denotes the beam power of the SVA algorithm. The array gain versus the number of receivers is simulated by uniform weighting, Hamming window weighting, CDA and SVA. The corresponding results are shown in Figure 8. The simulation results clearly demonstrate that the AG of the uniform weighting method yields a $10\log_{10}(N)$ theoretical curve, while the AG of the Hamming window weighting method decreases. Nevertheless, compared with the uniform weighting method, the AG of the SVA method slightly increases by approximately 0.5 dB.

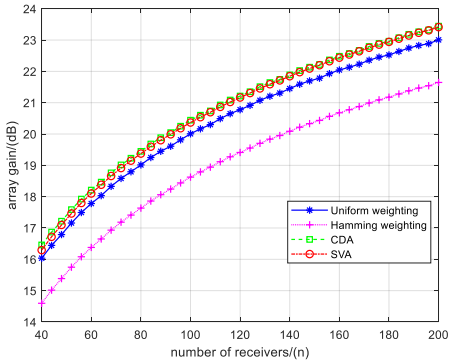

Figure 8. Comparison of the array gain versus the number of receivers.

4.1.3. Analysis of the quality of sonar images

The FLS array is composed of a transmitter and a 64-receiver ULA. The transmitted pulse is LFM with a bandwidth of 8 kHz and a pulse length of 40 ms. The two-dimensional uniform weighting separately method, two-dimensional cosine window weighting separately method, and one-dimensional two-step SVA are processed, and sonar images are achieved. Additionally, the angular dimension slice and range dimension slice of sonar images are obtained.

The 2-D sonar images and the target slices are shown in Figure 9. Figure 9a shows the sonar image when the angular and range dimensions are weighted by the uniform method separately. Notably, the sidelobe levels in the two dimensions around the targets are higher, causing the target images to be blurry. Figure 9b presents the image result obtained by the angular and range dimensions Hamming function weighted, where the sidelobe levels are suppressed at the expense of seriously decreased resolutions. Figure 9c shows a sonar image obtained by the proposed method, in which the sidelobe levels around the targets are thoroughly reduced to -40 dB while maintaining the resolution unchanged in two dimensions, resulting in enhanced targets. Furthermore, Figures 9d and e show the angular slice and range slice of the sonar images at the target, where the sidelobe levels in two dimensions are -40 dB on the premise of the main lobe width remaining unchanged.

Preprints (www.preprints.org) | NOT PEER-REVIEWED | Posted: 4 December 2023 doi:10.20944/preprints202312.0150.v1

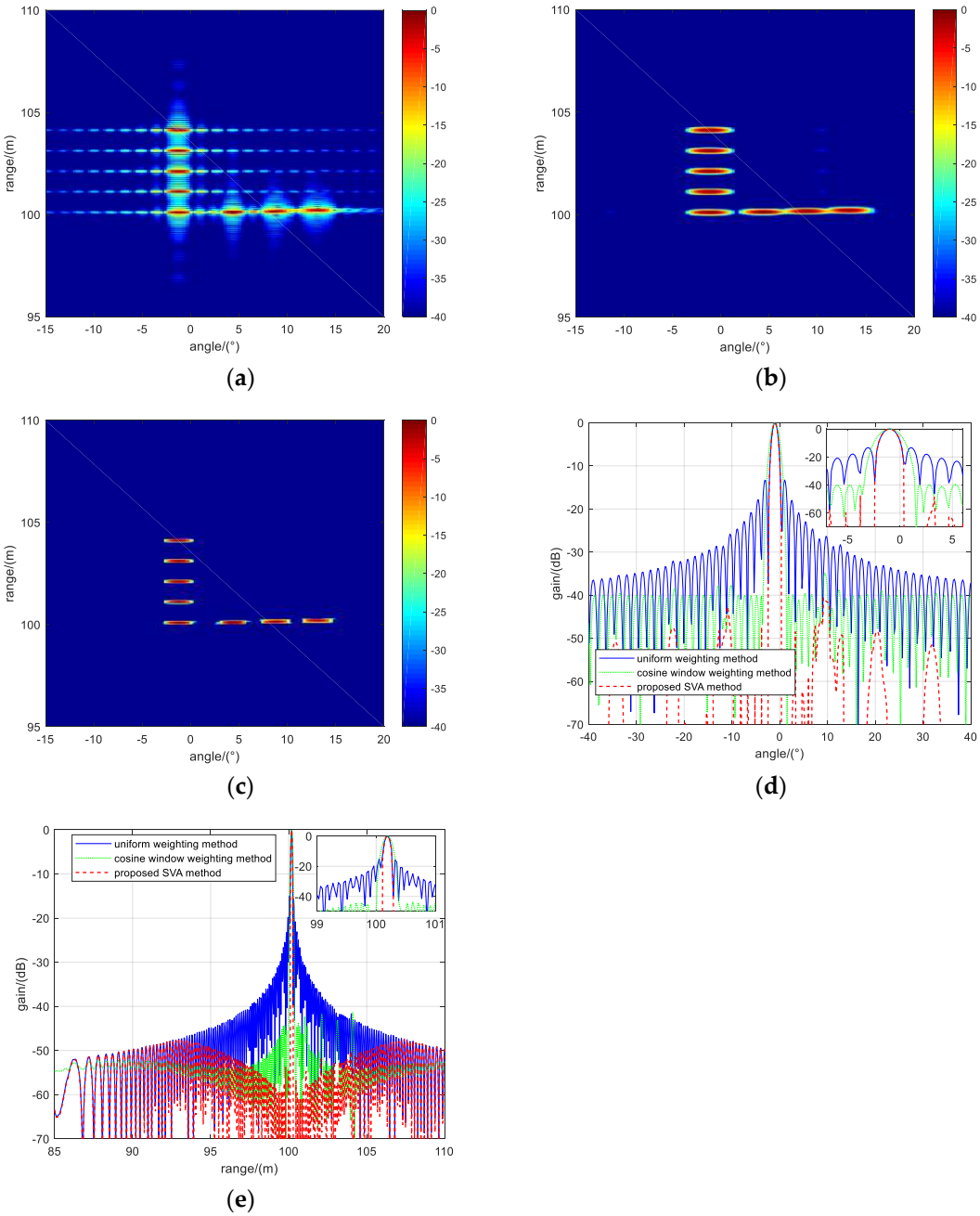

Figure 9. Comparison of the 2D acoustic images with different processing methods: **(a)** simulation image obtained by the uniform weighting method; **(b)** simulation image obtained by the Hamming window weighting method; **(c)** simulation image obtained by the proposed method; **(d)** results in the angular dimension corresponding to a target at 104 m; **(e)** results in the range dimension corresponding to a target at 12°.

4.1.4. Analysis of the computation burden

To analyze the computational burden of the proposed method, the computational times of the conventional uniform weighting method, cosine window weighting method and one-dimensional two-step SVA method are given in Figure 11, and the matrix size of the raw image is 256×1667 . The computer that was used is a PC with Intel (R) Core (TM) i7-10510U CPU @ 1.8 GHz, and the computation times are obtained by the MATLAB functions CLOCK and ETIME.

In Figure 10, the repeat run number is 50, and it is averaged. When the sonar array number is 100, the computation times of the two conventional window weighting methods measured approximately 0.4 s are basically the same. The one-dimensional SVA sequential processing method

Preprints (www.preprints.org) | NOT PEER-REVIEWED | Posted: 4 December 2023 doi:10.20944/preprints202312.0150.v1

is the post-processing of the raw image data with extremely simple computations, and the calculation amount is slightly higher than that of the conventional methods, so the proposed SVA method is particularly suitable for real-time imaging.

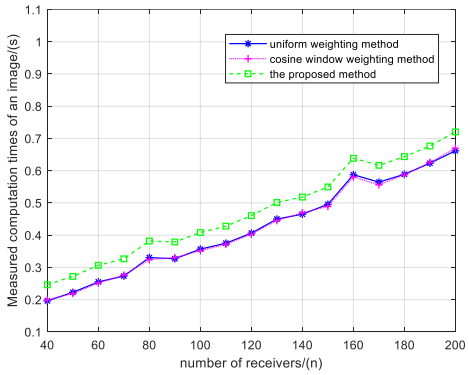

Figure 10. Comparison of the computing time with forming a raw image.

4.1.5. Analysis of the robustness

In this simulation, the amplitude and phase errors in the angular dimension of the system and the environmental errors are considered. Assuming that a receiving ULA of 80 elements is a spaced half wavelength, the array amplitude and phase errors are Gaussian distributed with variances equal to (1 dB, 5°) and (2 dB, 10°), respectively. The output beamforming is shown in Figure 11.

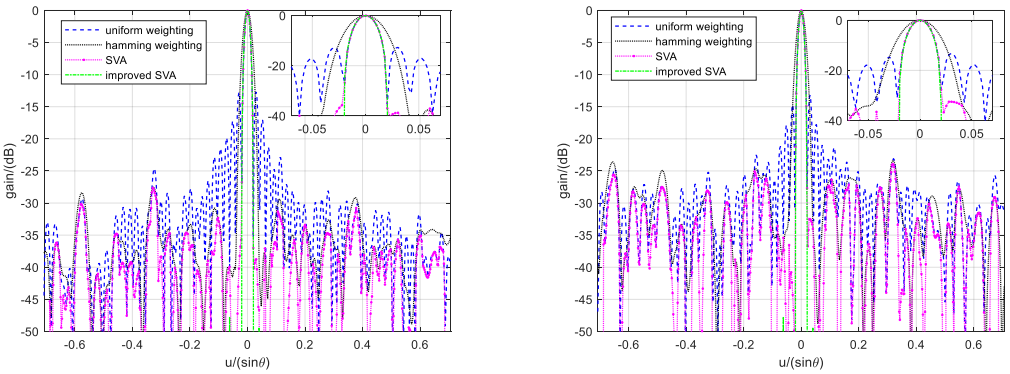

Figure 11. Comparison of the beam patterns under different amplitude and phase errors: (**a**) simulation results under amplitude and phase errors (1 dB, 5°); **(b)** simulation results under amplitude and phase errors (2 dB, 10°).

As shown in Figure 11, the performance of the window weighting methods and SVA method decreases with beam sidelobe levels higher than -30 dB when there are array amplitude and phase errors. However, the proposed improved SVA method combining the amplitude and phase error calibration method with the SVA method is not sensitive to the amplitude and phase errors, and the main side lobe ratio of the beam pattern is greater than 40 dB, which indicates good robustness.

4.2. Lake experimental data processing results

A lake experiment for forward looking imaging sonar was conducted to evaluate the proposed improved SVA method. The water depth in the experimental area was approximately 65 m. In this part, first, the array amplitude and phase errors are analyzed and calibrated. Then, the improved sonar images are obtained with low sidelobes and unchanged resolution by process experimental

Preprints (www.preprints.org) | NOT PEER-REVIEWED | Posted: 4 December 2023 doi:10.20944/preprints202312.0150.v1

data using the improved SVA method. The sonar system is suspended from an anchored ship, which is composed of a transmitter and an 80-receiver ULA.

4.2.1. Analysis of the array amplitude and phase error calibration

The sound source is placed underwater at the same depth as the sonar array with a horizontal distance of approximately 111 m, and the view of the lake calibration experiment is shown in Figure 12. The sound source emission signal is a single-frequency short pulse when the direct wave is selected for analysis and processing.

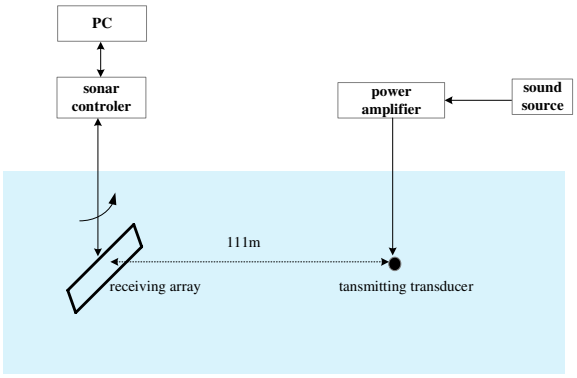

Figure 12. The view of the lake calibration experiment.

Based on the position of the sound source, the least squares estimation method is used to estimate the phase errors and amplitude errors. Then, the beam output performances of the uniform weighting method, Chebyshev weighting method, and improved SVA method before and after amplitude and phase error calibration are compared, and the results are shown in Figure 13.

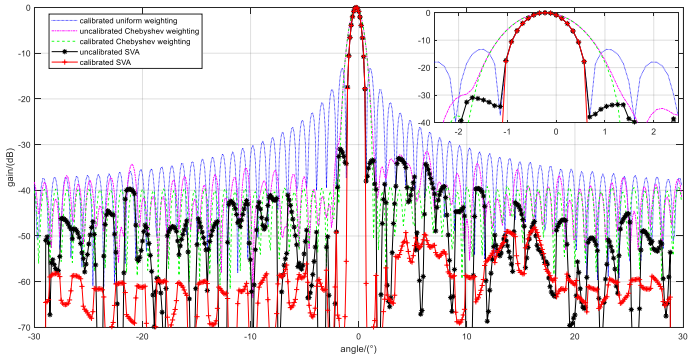

Figure 13. Comparison between the beam response of the uncalibrated array and the calibrated array.

Figure 13 shows that the calibrated beam pattern envelope is closer to the sinc function and the beam sidelobe levels are lower using uniform weighting. Moreover, the sidelobe levels are lower (-40 dB) after calibration but with main lobe width widening. For SVA filtering processing, the beam sidelobe levels after calibration are all below -45 dB, and the azimuth resolution remains unchanged.

4.2.2. Improved SVA method for data processing and analysis

The transmitted signal of the FLS is an LFM pulse, and the receiving array mainly receives the reflected echoes of targets and mountains in the water. The layout and scene of the lake experiment are shown in Figure 14. After calibrating the amplitude and phase errors of the array echo signal, the conventional imaging method, the azimuth-range Hamming window weighting imaging method,

Preprints (www.preprints.org) | NOT PEER-REVIEWED | Posted: 4 December 2023 doi:10.20944/preprints202312.0150.v1

and the azimuth-range two-step SVA imaging method are used. The imaging results are shown in Figure 15.

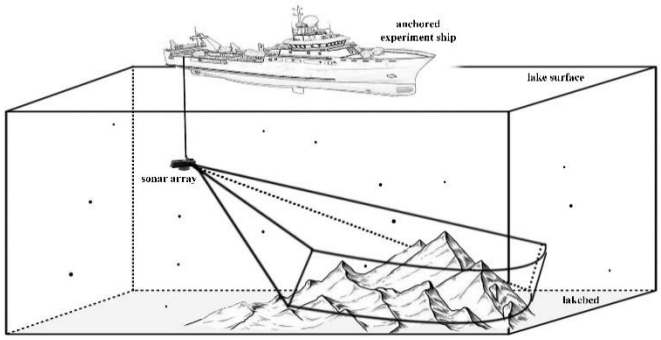

Figure 14. Lake experiment diagram.

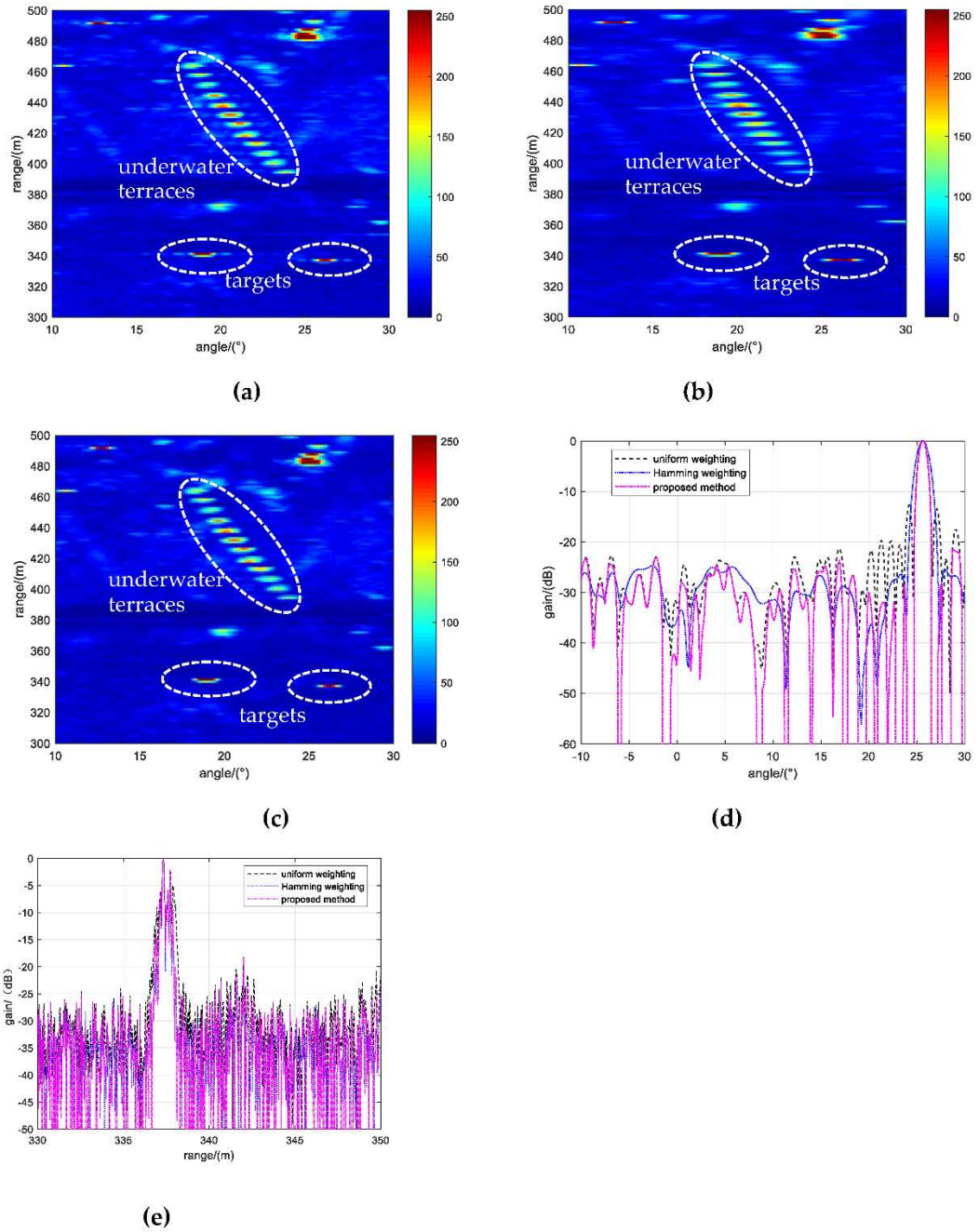

 doi:10.20944/preprints202312.0150.v1

Figure 15. The 2D images of sonar with different processing methods for sidelobe suppression: **(a)** FLS image obtained by the uniform weighting method; **(b)** FLS image obtained by the Hamming window weighting method; **(c)** FLS image obtained by the proposed method; (**d)** results in the angular dimension corresponding to a target at 337 m; **(e)** results in the range dimension corresponding to a target at 26°.

Figure 15 shows the sonar images of underwater mountains and underwater targets processed by the three methods. Compared to the sonar image obtained by the conventional method in Figure 15a, the sonar image generated by the proposed method in Figure 15c has a two-dimensional resolution approximately equal to that in Figure 15a and effectively suppresses the azimuth-range dimension sidelobe levels with sidelobe levels approximately equal to those in Figure 15b. Furthermore, Figure 15d shows the azimuthal section of the underwater target at a distance of 337 m, and the beam main lobe width remains unchanged at approximately 0.9°. Due to the influence of underwater reverberation and noise, the beam sidelobe levels near the target point are approximately -30 dB. Figure 15e shows the range dimension of the underwater target at an azimuth of 26°. At the same time, the proposed method partly reduced the sidelobe levels near the target point. However, with the influence of the high complexity of underwater acoustic channel propagation and frequency fluctuation characteristic of tansmitting-receiving transducers, the echoes LFM waveforms deviate from theoretical waveforms, so that the range dimension sidelobe suppression effect of the SVA method is not obvious in practice. Further research on the impact of underwater acoustic channel propagation on the emission waveform can be carried out to improve the algorithm. The above analysis shows that two-dimensional lower sidelobe level sonar images with unchanged azimuth-range resolution are obtained by using an improved imaging method, in which the sonar imaging performance is improved and beneficial for subsequent target detection and recognition.

5. Conclusions

Generally, the cosine window function weighting method is often used to reduce sidelobe levels for forward-looking sonar systems. This method has a lower computational cost and robustness, but it worsens the main lobe resolutions. To solve this problem, we first deduced the two-step SVA method to the forward looking sonar and improved the robustness to suppress the sidelobes without degrading the main lobe resolution in angular-range dimensions. We have shown, via theoretical analyses, numerical simulations and lake experiment results, that the improved spatially variant apodization algorithm can adequately improve the image quality by greatly reducing the sidelobes to approximately -40 dB on the premise of the main lobe width remaining unchanged. This process is extremely simple computationally. Due to the complex underwater environment, the propagation and variation characteristics of echoes in the range dimension will be studied through further research.

Author Contributions: Conceptualization, J.Y. and F.X.; methodology, L.Y. and F.X.; software, L.Y.; supervision, S.P. validation, L.Y. and S.P.; formal analysis, S.P.; investigation, J.Y.; data curation, F.X.; writing—original draft preparation, L.Y.; writing—review and editing, J.Y., F.X. and S.P.; funding acquisition, L.Y. All authors have read and agreed to the published version of the manuscript.

Funding: This work was funded by the IACAS Frontier Exploration Project under grant QYTS202107 and National Key Research and Development Program of China under grant 2022YFC2806101.

Data Availability Statement: The data presented in this study are available on request from the corresponding author. The data are not publicly available due to privacy or ethical restrictions.

Conflicts of Interest: The authors declare no conflict of interest.

References

1. Murino, V.; Trucco, A. Three-dimensional image generation and processing in underwater acoustic vision. Proc IEEE 2000.**2000**, 88,1903-1946.
2. Wang, S.; Wang, P.; Zhao, S.; et al. Feature-enhanced beamforming for underwater 3-D acoustic imaging. IEEE J. Ocean. Eng. **2023**,48,401-415.

3. Petillot, Y.;Ruiz, T. I.; Lane, D.M. Underwater vehicle obstacle avoidance and path planning using a multi-beam forward looking sonar. IEEE J. Ocean. Eng. **2001**,26,240-251.
4. Zhou, T.; Si, J.K.;Wang,L.Y.; et al. Automatic detection of underwater small targets using forward-looking sonar images. IEEE Trans. Geosci. Remote Sens. 2022,60, 4207912.
5. Kiang, C.W. ; Kiang, J.F.. Imaging on underwater moving targets with multistatic synthetic aperture sonar. IEEE Trans. Geosci. Remote Sens. **2022**,60, 4211218.
6. Thomas C, W. A CFAR detection approach for identifying gas bubble seeps with multibeam echo sounders. IEEE J. Ocean. Eng. **2021**,46,1346-1355.
7. Liu, X.H.; Fan, J.H.; Sun, C.; et al. High-resolution and low-sidelobe forward-look sonar imaging using deconvolution. Appl.Acoust.**2021**,178, 107986.
8. Wang, P.; Chi, C.; Liu, J.Y.; et al. Improving performance of three-dimensional imaging sonars through deconvolution. Appl.Acoust. **2021**,175, 107812.
9. Van Trees, H.L. Optimum array processing: part 4 of detection, estimation, and modulation theory. John Wiley & Sons Inc., New York, USA, 2002, pp. 17–79.
10. Fredric J, H. On the use of windows for harmonic analysis with the discrete Fourier transform. Pro. IEEE,**1978**,66,51-83.
11. Yan, L.; Piao, S.C.; Xu, F. Orthogonal waveform separation in multiple-input and multiple-output imaging sonar with fractional Fourier filtering. IET Radar, Sonar Navig. **2021**,15,471-484.
12. Ma, C.; Sun, D.J.; Mei, J.D.; et al. Spatiotemporal two-dimensional deconvolution beam imaging technology. Appl. Acoust. **2021**,183, 108310.
13. Stoica, P.; Wang, Z.; Li, J. Robust Capon beamforming. IEEE Signal Process. Lett. **2003**, 10,172-175.
14. Lønmo, T.I.B.; Austeng, A.; Hansen, R.E. Improving swath sonar water column imagery and bathymetry with adaptive beamforming. IEEE J. Ocean. Eng. **2020**,45,1552-1563.
15. Buskenes, J.I.; Hansen, R.E.; Austeng, A. Low-complexity adaptive sonar imaging. IEEE J. Ocean. Eng. **2017**,42,87-96.
16. Blomberg, A.E.A. Adaptive beamforming for active sonar imaging. doctor, University of Oslo, Oslo ,Norway,2011.
17. Liu, J.; Gershman, A.B.; Luo,Z.Q.; et al. Adaptive beamforming with sidelobe control: a second-order cone programming approach. IEEE Signal Process. Lett. **2015**, 10,331-334.
18. Gerstoft, P.; Xenaki, A.; Mecklenbräuker, C.F. Multiple and single snapshot compressive beamforming. J. Acoust. Soc. Amer. **2015**,138,2003-2014.
19. David, G.; Robert, J.I.; Zhang, B.; et al. Time domain compressive beam forming of ultrasound signals. J. Acoust. Soc. Amer. **2015**,137,2773-2784.
20. Guo, Q.J.; Yang,S.Y.; Zhou, T.; et al. Underwater acoustic imaging via online bayesian compressive beamforming. IEEE Geosci. Remote Sens. Lett. **2022**,19, 4024505.
21. Guo, Q.J.; Xin, Z.N.; Zhou, T.; et al. Adaptive compressive beamforming based on bi-sparse dictionary learning. IEEE Trans. Instrum. Meas. **2022**,71, 6501011.
22. Yang, T.C. Deconvolved conventional beamforming for a horizontal line array. IEEE J. Ocean. Eng. **2018**,43,160-172.
23. Yang, T.C. Deconvolution of decomposed conventional beamforming. J. Acoust. Soc. Amer. **2020**,148,195-201.
24. Guo, W.;Piao, S.C.; Yang, T.C.; et al. High-resolution power spectral estimation method using deconvolution. IEEE J. Ocean. Eng. **2020**,45,489-499.
25. Mei, J.D.; Pei, Y.Q.; Zakharov, Y.; et al. Improved underwater acoustic imaging with non-uniform spatial resampling RL deconvolution. IET Radar Sonar Navig. **2020**, 14,1697-1707.
26. Sun, D.J; Ma, C.; Mei, J.D.; et al. Improving the resolution of underwater acoustic image measurement by deconvolution. Appl. Acoust. **2020**,165, 107292.
27. Liu, X.H.; Yang,Y.X.; Sun,C.; et al. High-angular- and range-resolution imaging using MIMO sonar with two-dimensional deconvolution. IET Radar Sonar Navig. **2023**,17,991-1001.
28. Stankwitz, H.C.; Dallaire, R.J.; Fienup, J.R. Spatially variant apodization for sidelobe control in SAR imagery. IEEE National Radar Conf., Atlanta,GA,USA,29-31 March 1994.
29. Stankwitz, H.C.; Dallaire, R.J.; Fienup, J.R. Nonlinear apodization for sidelobe control in SAR imagery. IEEE Trans. Aero.Electron. Syst. **1995**, 31,267-279.
30. Zhu, R.Q.; Zhou, J.X.; Fu,Q. Spatially variant apodization for sidelobe suppression in near range radar imagery. IET Radar, Sonar Navig. **2022**,16,986-999.
31. Ding, Z.G.; Zhu, K.W.; Wang, Y.; et al. Spatially variant sidelobe suppression for linear array MIMO SAR 3-D imaging. IEEE Trans. Geosci. Rem. Sens. 2**022**,60, 5220915.

 doi:10.20944/preprints202312.0150.v1

disclaim responsibility for any injury to people or property resulting from any ideas, methods, instructions or products referred to in the content.